D4.1 – Electronic skin with 7-10 sensors and readout circuit

Project Number: 965044

Project Acronym: B-CRATOS

Project Title: Wireless Brain-Connect inteRfAce TO machineS

This project has received funding from the European Union's Horizon 2020 research and innovation programme under grant agreement No 965044

Deliverable Information

Project Title:	Wireless Brain-Connect inteRfAce TO machineS (B-CRATOS)
Project Number:	965044
Deliverable Number:	D4.5 e-skin with 7-10 sensors and readout circuit
Responsible Partner:	Uppsala University
Work Package Number and Title:	WP4 Design and integration of the biomechatronic prosthetic upper limb
Task Number and Title:	T4.2 Artificial skin
Version:	3
Revision Date:	20-09-2023

Dissemination Level: Public

Approvals

Name, Org.	Role	Signature	Date
Libo Chen	Author	Libo Chen Digitally signed by Libo Chen DN: cn=Libo Chen, c=SE, o=Uppsala universitet, ou=Inst. för elektroteknik; Fasta tillståndets elektronik, email=libo.chen@angstrom.uu.se Date: 2023.09.20 10:35:22 +02'00'	2023-09-20
Zhibin Zhang	Author	Zhibin Zhang	2023-09-20
Robin Augustine, UU	Project Coordinator	Robin Augustine	2023-09-20

This project has received funding from the European Union's Horizon 2020 research and innovation programme under grant agreement No 965044

Executive Summary

This document reports the activities for the design and assessment of a novel neuro-inspired electronic (e-) skin that advances the previous work in the capability of encoding dynamic tactile information. Conducted by UU, we applied the neuromorphic approach to develop a theoretical model of the new e-skin to guide the design of the circuit. To assess the design, an array of 8 Cu-electrodes for sensing in a finger-shaped flexible substrate was fabricated. Characterizations of sensing operation, signal processing and the encoding of information were performed. It is evidenced that our neuromorphic approach advances the previous work by demonstrating the e-skin has the capability of coding dynamic tactile events in an energy-efficient manner. Subsequently, arrays of hydrogel-based mechanical sensors fabricated directly on MIA fingers were assessed and characterized. To enable the e-skin on MIA fingers to capture the most crucial contact information, we tailored our circuit design to enable the sensor array to preferentially encode the information about the onset of contacting events. Statistical characterizations of individual sensors show the input-output relation, response range and sensitivity, and robustness against variation of materials in contact. In addition, we studied encoding tactile information in a population of 8 sensors, which reveals the distinct patterns of object properties in stiffness and curvatures encoded in spike trains. Our breakthrough has paved the way for e-skin development with the ultimate goal of human-like tactile perception.

This project has received funding from the European Union's Horizon 2020 research and innovation programme under grant agreement No 965044

Table of Contents

This project has received funding from the European Union's Horizon 2020 research and innovation programme under grant agreement No 965044

1 Overview

1.1 Purpose

This document aims to report achievement and results of our design of a novel neuro-inspired e-skin to go beyond of the state of art. Assessment of the design was performed using an e-skin containing 8 Cu-electrodes. We show that employment of TENG-based single-electrode tribotronic transistor as tactile sensor results in energy efficient sensing operation and ease of fabrication, but suffers from unwanted variations upon repeating contacts. The issue is effectively resolved by neuromorphic signal processing in hardware. When the new e-skin is applied onto MIA fingers by incorporating hydrogel-based sensing electrodes into artificial skin, a method to facilitate tuning signal output of multiple sensors was developed. Response of sensors on MIA fingers to contact events with different force up to 70 N, contact speed and contact materials were characterized.

1.2 B-CRATOS Partners

Short Name	Full Name
UU	Uppsala Universitet
SINANO	Institute Sinano Association
SSSA	Scuola Superiore di Studi Universitari e di Perfezionamento S'Anna
BRME	Blackrock Microsystems Europe GmbH
LINKS	Fondazione LINKS – Leading Innovation & Knowledge for Society
DPZ	Deutsches Primatenzentrum GmbH
NTNU	Norges Teknisk-Naturvitenskapelige Universitet NTNU

1.3 Responsibilities

SSSA is the lead beneficiary responsible for the WP 4.
UU is the lead beneficiary responsible for Task 4.2 and Deliverable 4.1. UU was the original responsible for the Deliverable 4.3, which was meant to include both the mechanical integration (under the responsibility of SSSA) and the electrical design of the sensor (under the
responsibility of UU). The consortium decided to split the two contributions such that SSSA focuses the deliverable 4.3 to the mechanical integration. UU includes the sensor design into

This project has received funding from the European Union's Horizon 2020 research and innovation programme under grant agreement No 965044

Deliverable 4.5 which presents the design, working principles, and electrical characterizations of the novel e-skin UU developed.

Prof. Robin Augustine (UU) is the scientific coordinator assuming overall project, scientific, and technical responsibility of the project. As B-CRATOS coordinator, Prof. Augustine reviews, approves, and submits deliverables and reports.

1.4 Definitions

Term	Description
TENG	Triboelectric nanogenerator
SNN	Spiking neural network
ML	Machine learning
PCB	Printed circuit board
PDMS	Polydimethylsiloxane
LIF	Leaky-integrate-and-fire
FET	Field-effect transistor

1.5 Key references

[1] Dale Purves, et.al., Neuroscience, Chapter 9, 5th Edition, 2012, Sinauer Associates

[2] Hochberg, L. R. et al. Reach and grasp by people with tetraplegia using a neurally controlled robotic arm. (2012) Nature 485, 372-375.

[3] Raspopovic, S., Valle, G. & Petrini, F. M. Sensory feedback for limb prostheses in amputees. (2021) Nat Mater 20, 925-939.

[4] Chen, L., et.al., Artificial tactile peripheral nervous system supported by self-powered transducers. (2021) Nano Energy 82, 105680

[5] Z.L. Wang, et.al., On the origin of contact-electrification, Materials Today, **30**, 34, 2019

[6] W. Gerstner et.al., Neuronal dynamics, Cambridge, ISBN 978-1-107-63519-7

[7] K. Bai, et.al., Opening the “Black box” of silicon chip design in neuromorphic computing, Bio-inspired technology, DOI: 10.5772/intechopen.83832

This project has received funding from the European Union’s Horizon 2020 research and innovation programme under grant agreement No 965044

2 Artificial skin for B-CRATOS system

2.1 Introduction

Tactile feedback, which plays a crucial role in human dexterity for object manipulation and haptic exploration, originates from the skin. The skin, the body's largest organ, houses a multitude of mechanoreceptors that come in four different types. These specialized cells envelop the endings of primary afferent fibers. When a tactile stimulus is applied, these mechanoreceptors transform the indentation of the skin into receptor potentials. These potentials, when they reach a sufficient magnitude, trigger action potentials, often referred to as "spikes," in the primary afferent neurons. Consequently, tactile signals are encoded into spike trains, which represent a temporal sequence of spikes. The precise timing of these spikes holds critical information. Following this encoding process, these spike trains are transmitted through a multi-stage afferent sensory pathway. This complex pathway is responsible for delivering the tactile information to the sensory cortex, where it can be further processed and interpreted [1].

When a patient experiences the loss of a sensory modality due to injury or disease, modern neural prostheses come to the rescue, aiming to restore the lost sensory function. Remarkable advancements have been achieved in the field of efferent brain-machine interfaces (BMI). These interfaces are designed to capture and translate neuronal information from the brain into commands that can control external devices such as computer cursors, wheelchairs, and robotic limbs [2]. These commands are often executed with the aid of visual feedback. However, when we compare this progress with the essential role that tactile feedback plays in guiding normal motor behavior, a significant gap becomes evident. The absence of tactile sensory feedback poses a significant challenge for the effective utilization of neuroprosthetic limbs. This limitation severely impedes the seamless integration and functionality of such prosthetic devices.

Electronic (-e) skin is a versatile and flexible electronic device covering a large area. It consists of sensor arrays that convert mechanical stimuli, such as force, into analog signals, typically in the form of voltage or current. Various mechanisms such as resistive or capacitive sensing have been applied [3]. However, the conventional method of reading out these analog signals poses significant limitations in practical applications. Firstly, when transmitting analog signals over longer distances, typically 1 meter from the e-skin on extremities to the brain, issues like signal drift and noise interference become significant concerns [4]. Secondly, the serial readout process introduces latency, especially when dealing with a high number of sensors. This latency can lead to the loss or distortion of tactile information, making it inadequate for rapidly changing tactile events like vibrations. While increasing the sampling speed and data rates can reduce latency, it also results in higher power consumption. Thirdly, current e-skin technologies suffer from substantial power consumption, even when not actively sensing stimuli. Additionally, the conventional readout circuits are inefficient in terms of power usage. Finally, there's a fundamental mismatch in signal type between e-skins and

This project has received funding from the European Union's Horizon 2020 research and innovation programme under grant agreement No 965044

the brain. The readout signals from e-skins are in analog form, whereas the brain communicates using spikes, or action potentials. This discrepancy further exacerbates latency and power consumption issues, especially as the number of sensors scales up, limiting the practical scalability of e-skin applications.

2.2 Architecture and requirements

As illustrated in Fig. 1, the biomimetic artificial skin under development comprises an array of tactile sensors that transduces a tactile stimulus (P(t)) into an analog electrical signal (voltage, V(t)), a neuromorphic circuit that converts V(t) into spikes, a temporal sequence of events denoted by delta function $\delta(t-t^f)$ where t^f is the moment in time of a spike. In order to interface the skin with the artificial intelligence (AI) board under development by LINKS, output high voltage (2V) for a spike and low voltage (0 V) for non-spike will be used.

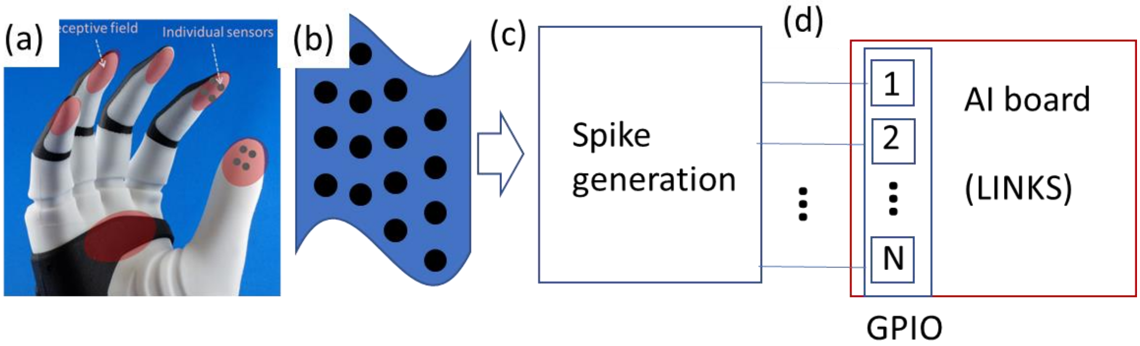

Fig. 1 An overview of the artificial skin. (a) Locations within the Mia Hand that will be developed by SSSA. It comprises (b) a sensor array that converts a mechanical stimulus into an analog electrical signal, voltage, (c) an analog electronic circuit that converts voltage into spikes.

Our original objective to develop a biomimetic device with the following requirements.
(1) we aim to create self-powered sensing of force ranging from 0 to 70 N with the sensitivity of >1 mV per µm of e-skin deformation. As we will show later, the sensitivity of >1 mV per µm of e-skin deformation has been reached.
Second, we aim to render the e-skin capable of discern textures with spatial resolution of at least 1 mm. The work to this objective is underway.
Third, we aim to enable the e-skin recognize materials. As we will show later, we have achieved this.
Finally, we aim at make the e-skin capable of being embedded in a compliant pulp moulded on the finger of the hand. This objective has been achieved as described in D4.3.

Below, we focus on the results of our e-skin development in the model, design, and performance in signal processing, as well as the electrical characterization of our e-skin technology integrated into MIA fingers.

This project has received funding from the European Union's Horizon 2020 research and innovation programme under grant agreement No 965044

3 Method and Results

This section aims to describe the design and implementation of the novel e-skin by means of the neuromorphic approach. We first build the theoretical model based on TENG mechanism for sensing and the computational neuroscience principles for signal processing. Subsequently, we implement the model by means of the PCB technology and assess the performance of individual sensors and population of a few sensors. The results show that the neuromorphic approach we applied leads to an e-skin capable of encoding dynamic information about contact events. Using TENG-based transducer is of energy efficiency but subject to unwanted variations occurred during repeating contacts. The issue can be effectively resolved by the neuromorphic approach for signal processing. Electrical assessment of TENG-based sensors with their sensing electrodes embedded in artificial skin on MIA fingers has been extensively performed. A method about how to efficiently tune individual sensors on MIA fingers was developed. Response of sensors on MIA fingers to contact events with different forces up to 70 N, contact speed and contact materials were characterized.

3.1 Our novel neuromorphic e-skin

3.1.1 The working principles of the new e-skin

- *The physical model*

We design the e-skin by mimicking tactile peripheral afferent neurons of which endings are receptors. As shown in Fig 1, the e-skin comprises an array of sensors and an electronic circuit for spike generation (an analog-to-spike converter). Let us assume that $\mathbf{P}(t)$ is a vector composed of physical quantities about a stimulus applied to the sensor array at a time moment t. For instance, the stimulus can be force, pressure, or distance between the object and the e-skin surface. $\mathbf{P}(t)$ is transduced to analog signal in the form of voltage, $\mathbf{V}(t)$, via an operator, $\boldsymbol{Tr}$. The $\mathbf{V}(t)$ is subsequently converted to spike trains, $\mathbf{ST}(t)$, via G.

$$\boldsymbol{Tr}: \boldsymbol{P}(t) \rightarrow \boldsymbol{V}(t) \qquad (1)$$

$$\boldsymbol{G}: \boldsymbol{V}(t) \rightarrow \boldsymbol{ST}(t) \qquad (2)$$

To implement (1), we employed the TENG-based transduction mechanism [5]. The TENG-based transducer harnesses the mechanical energy for the transduction, ruling out the necessity of constant power supply as required for the resistive and capacitive sensors. Therefore, it is a self-powered transducer. As reported in D4.1, the transducer we designed is of one electrode connected to the gate terminal of a transistor, which is called one-electrode tribotronic transistor.

As described in our previous publication [4], about the relation between the open-circuit potential generated in the TENG-based sensor Φ and the distance d between a plane-like

This project has received funding from the European Union's Horizon 2020 research and innovation programme under grant agreement No 965044

object and the surface of an artificial skin, we have $\Phi=\Phi(\mathrm{d})$, where Φ is influenced by surface charge density on the object (σ_T) and skin surface (σ'_T). Here, the stimulus is expressed as the distance d. When d>0 and is small, an appreciable increase of Φ suggests a detection of the proximity of the object by the sensor. When $d<0$, the response in the Φ is resulting from skin deformation caused an applied force. One has to note that by multiple physical contact, contact electrification may induce a change of σ_T, which causes a change in the. To readout information about d, one has to incorporate a load which converts Φ to V.

Upon $V(t)$ on a load circuit, current I_i is generated, which drives the analog-to-spike converter to generate spike trains. The signal conversion is realized via a process governed by the LIF neuron model. The LIF model states that a state variable of the converter which is called the membrane potential V_i

$$\tau_{mem}\frac{dV_i(t)}{dt} = -(V_i(t) - V_{rest}) + RI_i(t) \qquad (3)$$

Whenever $V_i(t) = \vartheta$, the threshold potential, a spike is generated and V_i is reset.

Here, τ_{mem} is the membrane time constant, R is the membrane resistance, V_{rest} is the resting potential.

- *Dynamic stimulation of the sensors upon interaction between object and e-skin*

Assuming there are M TENG-based sensors, they are labelled with integers, 1, 2, …, M. A sensor is labelled with a_i which belongs to the set of labels. For a single object-hand interaction that progresses from the moment of initial contact (t=0) to time t, suppose there are $l(t)$ sensors that have been sequentially stimulated in the duration between 0 and t. The activated receptors ordered in the stimulation sequence comprise a permutation

$$SR^S = (a_i \,|\, i=1, \cdots, l(t)), \qquad a_{l(t)} \leq M \qquad (4)$$

The increase in i with time t and the order of the activated sensors correlate with the dynamic interaction between the object and the e-skin.

- *Dynamic transduction of tactile stimuli into voltage*

When the interaction between the object and the e-skin progresses to time t after the initial contact, l sensors are sequentially stimulated in the period $0 \leq t' \leq t$. The stimulus applied into a sensor a_i at time t' is expressed as $P_{ai}(t')$. We construct a vector of the stimulus $P_{ai}(t')$ for all activated sensors as

$$\boldsymbol{P}(t') = \langle P_{ai}(t') \,|\, a_i \in SR^S \rangle, \qquad 0 \leq t' \leq t \qquad (5)$$

The stimulus $\boldsymbol{F}(t')$ is transduced into voltage via the TENG mechanism, $\boldsymbol{Tr}$, as

This project has received funding from the European Union's Horizon 2020 research and innovation programme under grant agreement No 965044

$\boldsymbol{V}(t') = \langle \boldsymbol{V}_{ai}(t') \mid a_i \in SR^S \rangle$, $0 \le t' \le t$ (6).

- *Signal conversion and neuromorphic encoding of dynamic tactile information*

The circuit converts the voltage into spikes following (1) and (3), which results in an ensemble of spike trains

$$\boldsymbol{ST}(t') = \left\langle ST_{a_i}(t') = \sum_{n=1}^{n=N_{a_i}(t)} \delta(t' - t_{a_i}^n) \,\middle|\, a_i \in SR^S \right\rangle, 0 \le t' \le t \qquad (7)$$

For $a_j \notin SR^S$, $ST_{a_i}(t') = 0$. Here $t_{a_i}^n$ is the timing of spike n ($n \ge 1$) fired in the activated artificial afferent a_i in the period $0 \le t' \le t$ and $N_{a_i}(t)$ the total number of spikes fired by the activated afferent a_i in the same period. The dimension of the delta function in equation (7) is t^{-1}. Note that the vector $\boldsymbol{ST}(t')$ encodes the tactile information in both spatial domain (i.e., a_i) and time domain (i.e., $t_{a_i}^n$). The purpose of our circuit design of the new e-skin is to implement the encoding tactile information in the spatio-temporal pattern (7).

3.1.2 Implementation and characterizations

To implement the coding (7), our strategy is to combine the TENG-based tactile sensors and an analog-to-spike converter based on the LIF model. The former is to transduce a physical quantity $\boldsymbol{P}$ representing a tactile simulation into an analog signal in voltage $\boldsymbol{V}$ while the latter is to convert $\boldsymbol{V}$ into spike trains. Here, one single TENG-based tactile sensor refers to one tribotronic transistor and the associated load circuit prior to the converter.

To fabricate an array of TENG-based tactile sensors, the sensing electrodes were formed by filling conductive hydrogels into cavities of a PDMS film or by patterning a Cu film on a polyimide film by means of the flexible PCB technology. An electrode is connected to the gate electrode of a transistor. For the Cu electrodes, a PDMS film was subsequently deposited onto the Cu/polyimide to mimic the skin. To prepare the PDMS film, the base and curing agent of silicone elastomer (Sylgard™ 184) were mixed in a weight ratio of 10:1, and degassed in the vacuum oven at room temperature. The mixture was evenly coated on the surface of the FPCB and cured at 80 °C for 8 h to form a uniform PDMS film with a thickness of ~500 µm. The PDMS film worked as the contact layer for triboelectrification.

The analog-to-spike converter was designed according to the LIF neuron model [7]. The circuit is analog in nature, instead of digital, which was designed and fabricated by using PCB technology. As shown in Fig 2, our simulation of the LIF neuron circuit successfully generates the LIF behaviour. When the membrane potential Vi hits a threshold during the accumulation due to the input current, a spike is generated. The operation is governed by the dynamic described by equation (3). The converter is powered by V_{DD} which is 5 V in this case. When an

This project has received funding from the European Union's Horizon 2020 research and innovation programme under grant agreement No 965044

object approaches the PDMS skin, both containing surface charges of different charge densities, the electrostatic induction leads to a change in the triboelectric potential V_T on the gate electrode. The transistor is turned on, allowing a current to flow through the channel of the transistor. The current is injected into the converter. Firstly, the current is integrated into a capacitor until the membrane potential V_i reaches the threshold ϑ. At that point, the output signal goes from zero to the power supply rail (2V in this case) to fire a spike. The accumulated charges on the capacitor leak to the ground~~,~~ and the membrane potential is reset to zero.

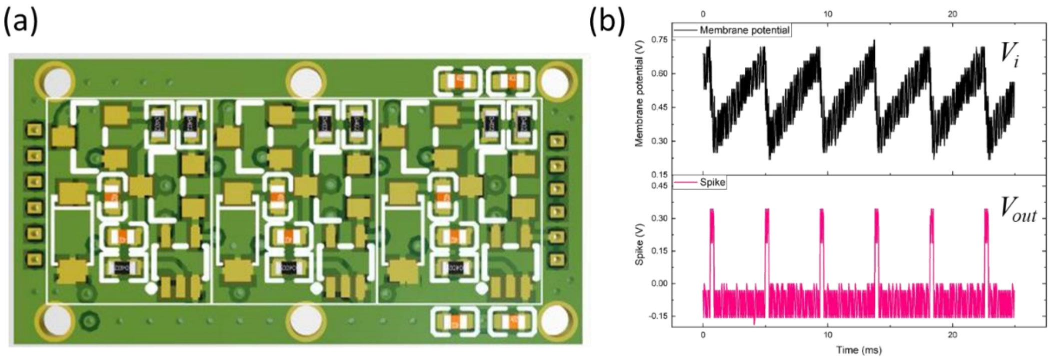

Fig 2. The circuit design of (a) analog-to-spike converter using the LIF model by means of the PCB technology which successfully generates (b) the LIF behaviour.

In order to shed light on the electrical response of a single tactile sensor to a physical contact, measurements of triboelectric voltage $\boldsymbol{V_T}$ on the gate electrode and spike trains $\boldsymbol{ST}$ from the converter were performed using a Shimadzu AGS to control the contact of an indenter on the sensor (Fig 3). An important measure we have taken is to enable simultaneous measurements of mechanical and electrical quantities by integrating our neuromorphic circuit (4) to the setup. During the execution of a contact event when the indenter moves to the sensor and retreats at a constant speed, the distance $\boldsymbol{d}$ between the surface of the indenter and the surface of the artificial skin, the force $\boldsymbol{F}$ which is applied to the artificial skin, the triboelectric potential $\boldsymbol{V_T}$ and spike trains $\boldsymbol{ST}$ were measured simultaneously.

As shown in Fig. 4 (a), the triboelectric potential $\boldsymbol{V_T}$ starts to rise as the indenter approaches a specific sensor (the red line) before physical contact is made. In this specific sensor, the response in V_T starts to occur when the intender is around 2mm away from the elastomer surface. The onset of the physical contact is associated with the moment when the force starts to rise (Fig4 (b)). Sensing the proximity is equivalent to an additional 2mm-thick air layer on the top of the artificial skin. On the other hand, the voltage changes with the force in the range of the force from 0 to 50 N, as denoted by the shadowed area. In the physical contact phase, the TENG-based tactile sensor has a good linearity as shown in Fig 4(c) for a specific sensor with hydrogel electrode embedded in a PDMS skin. In the proximity, the change in the voltage is around 0.8 V for a change in the distance of 1mm, i.e., the sensitivity of this phase is 0.8 mV/μm. In the physical contact phase, the sensitivity of this specific sensor

This project has received funding from the European Union's Horizon 2020 research and innovation programme under grant agreement No 965044

is around 0.4 mV/µm. From the relation between the strain and stress, the sensitivity is also expressed as around 1.5 mV/kP.

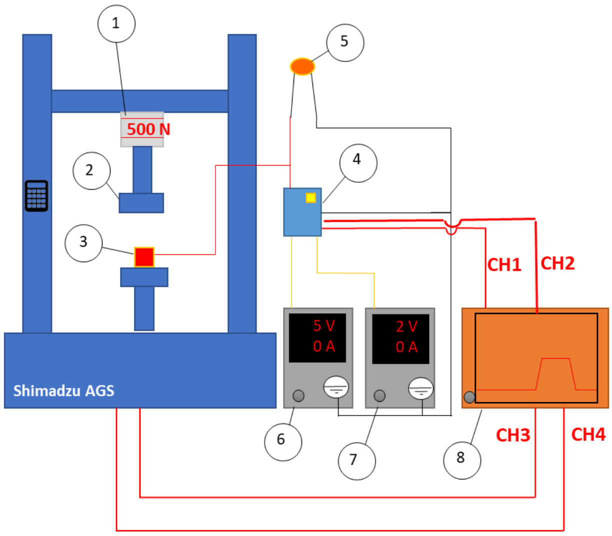

1. Load cell
2. Flat indenter
3. Specimen
4. PCB
5. Capacitor load
6. Power supply for voltage amplitude modulation output
7. Power supply for frequency modulation output
8. Oscilloscope
9. CH1: spike trains (ST)
10. CH2: VT
11. CH3: Force output from AGS
12. CH4: distance output from AGS

Fig 3. The setup for simultaneous mechanical and electrical measurements using a Shimadzu AGS to control contacts.

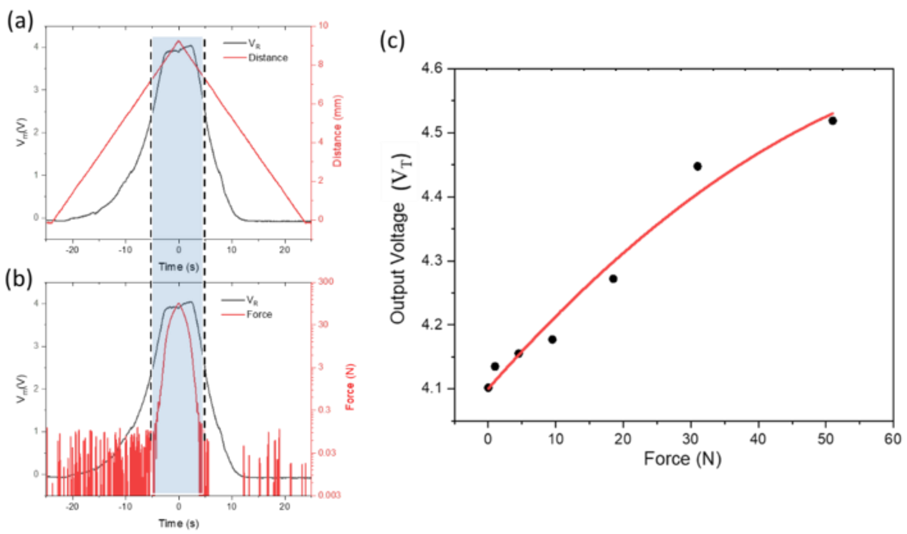

Fig 4. Electrical output in voltage of a typical sensor in response to stimulation characterized by (a) indenter-skin surface distance and (b) force arising from the physical contact between the indenter and the sensor, as well as (c) the relation between the output in voltage and force.

This project has received funding from the European Union's Horizon 2020 research and innovation programme under grant agreement No 965044

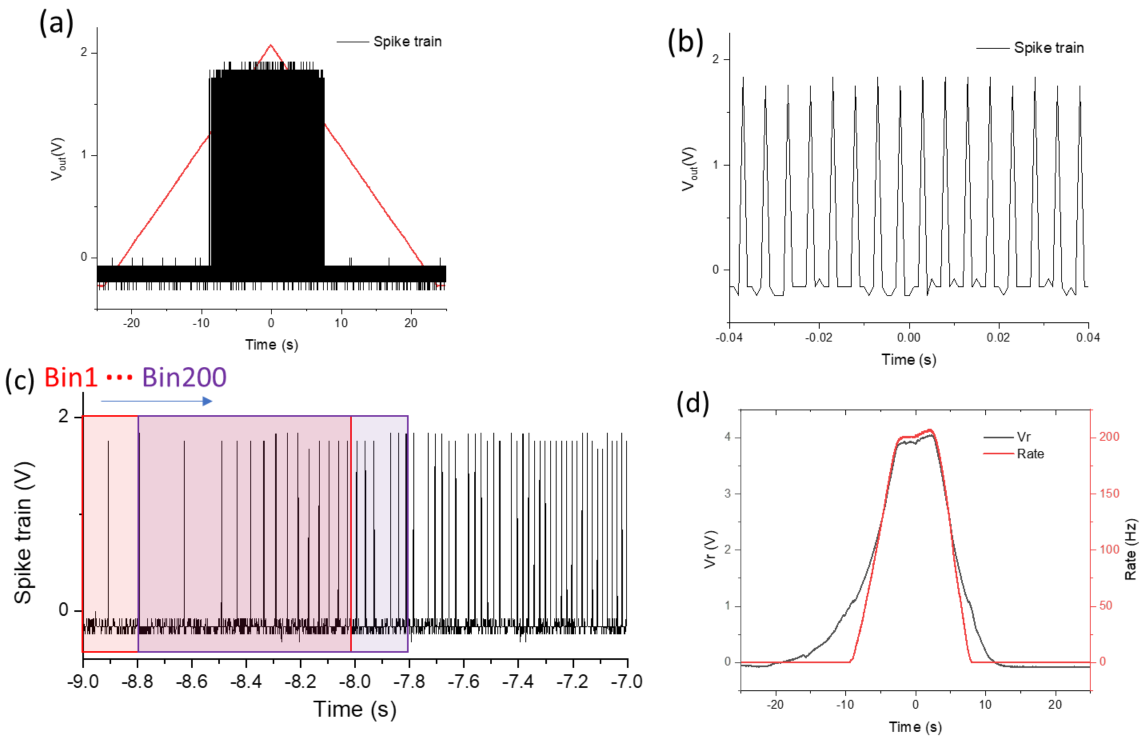

Fig 5. (a) Output in spikes from analog-to-spike converter and (b) zoom of the spikes in response to an indenter-sensor contact, (c) the method to calculate instantaneous spiking rate by shifting a bin (width of 1 s) with a step of 0.1 ms a time along a spike train and (d) comparison between voltage and spiking rate in encoding the tactile information of an indenter-sensor contact.

Through the analog-to-spike converter, a spike train was obtained as shown in Fig 5 (a). As obtained by oscilloscope, the spike train is analog in nature, Fig 5 (b). The rapid change in voltage gives rise to typical spike features with an amplitude at 2 V and a width 1.2 ms. In the circuit design, the amplitude is tunable. It can be set to be 0.1 V as the amplitude of action potential. Here it was set to be 2 V in order to be compatible with the requirements of the AI board developed by LINKS. Each spike is featureless and represents an event. As being described earlier in the theoretical model, the timing of the spikes encodes tactile information. The encoding of information can also be in the inter-spike interval (ISI) in time. If one defines a time window (i.e., bin) with a span of e.g., 1s, one can get a variable of spiking rate by counting the total number of spikes in the window normalized to the length of the time window which has a unit of Hz. When the bin is shifted along the time course by 1 ms a time, one can obtain a time-dependent spiking rate (Fig 5 (c)). As shown in Fig 5(d), when V_T has already increased when the indenter is around 2mm from the elastomer skin surface, the spiking rate stays at zero. The spiking rate starts to rise only when the indenter is around 1

This project has received funding from the European Union's Horizon 2020 research and innovation programme under grant agreement No 965044

mm away from the elastomer surface, as compared with V_T which starts to rise at 2mm. It deserves to be mentioned that one actually cannot discern any difference simply by using the electrical response to sense the contact. However, it is important to identify the moment when an initial physical contact is made for tactile feedback required in object manipulation.

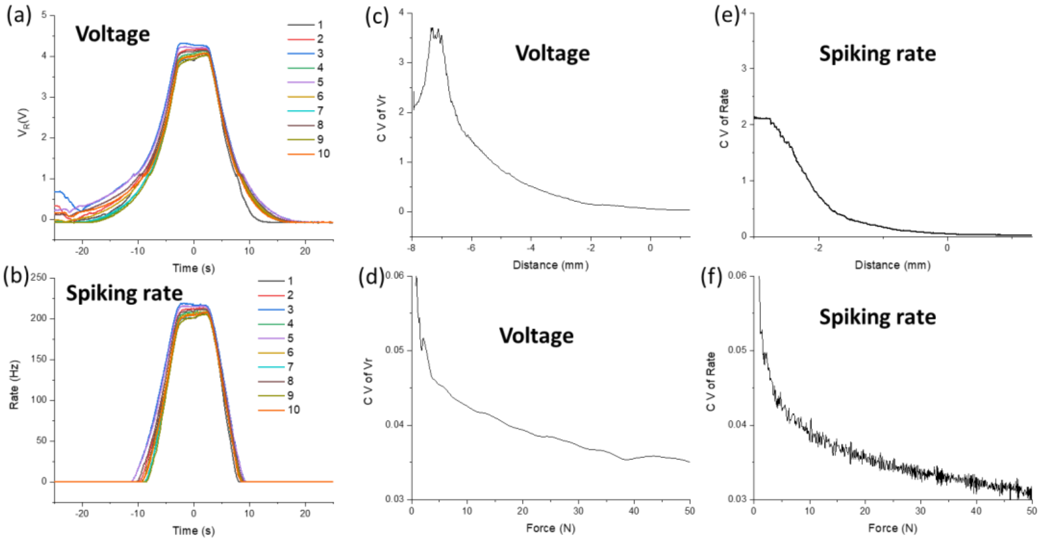

Fig. 6. The time courses of (a) V_T and (b) spiking rate upon repeated contacts as well as (c-f) the coefficient variations of V_T and spiking rate.

One distinct advantage of using spikes to represent tactile information is an enhanced robustness against variations caused in repeating contacts. As shown in Fig 6 (a) where the time courses of electrical responses were recorded upon repeating contacts, it is observed that the variation of V_T has been relatively substantial when the indenter is in a larger distance from the elastomer surface, which is obviously unwanted. It is assumed that the variations may be originated from the contact electrification to cause variations in the surface charge densities on the two surfaces during physical contacts. As a contrast, the unwanted effect does not appear as the response in spiking rate at the long distances has been completely suppressed (Fig 6(b)). In addition, the variation of spiking rate is relatively smaller than that of V_T in the proximity and the physical contact phases. This is evidenced by relatively smaller coefficient of variation (C.V.) of spiking rate as shown in Fig 6(c-f). In Fig 6 (c), V_T increases with a large variation characterized by C.V. of 3.5 when the object is 8 mm away from the skin surface. As a comparison, the spiking rate starts to increase when the object is 3 mm away from the skin surface with a relatively smaller C.V. of 2. Furthermore, in the physical contact phase when a force is applied, the values of C.V. for the spiking rate is relatively smaller than that of V_T.

As mentioned, it may be significant for dexterous object manipulation to discern the moment when physical contact occurs. The question is how one can identify such a critical moment when the proximity effect is present. The answer lies in the first derivatives of the

This project has received funding from the European Union's Horizon 2020 research and innovation programme under grant agreement No 965044

variables. Fig 7(a) depicts the time courses of V_T and its derivative. In Fig 7(b), it shows that the peak of the derivative occurs at the same time with that of the force to rise from zero. Similarly, the derivative of the spiking rate can be used to locate the moment of the physical contact (Fig 7(c) and (d)).

It deserves to stress that our conductive hydrogel, as it is based on the Li-based electrolyte, is relatively electro-chemical reactive. The electrochemical reactivity corrodes Cu wires in a long-time span. We found that the Cu wires with Ag coating has a resistance against the chemical corrosion. On the other hand, the electro-chemical reaction can be stimulated at sufficiently high voltage. It indicates that the induced triboelectric voltage upon repeated contacts speeds up the corrosion of the wires.

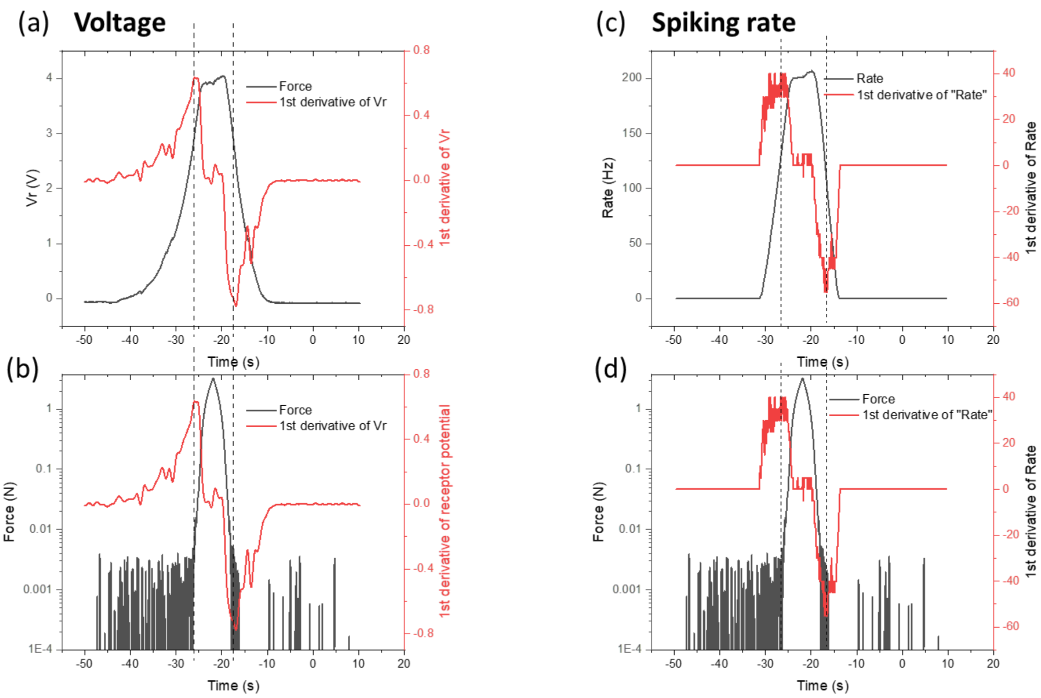

Fig 7. The first derivative of VT (a) calculated from the time course of VT (b) determining the onset of the physical contact, and (c) the first derivative of spiking rate from the time course of spiking rate (d) determining the onset of the physical contact.

3.1.3 Investigation of sensing and coding in population

We have fabricated an e-skin comprising 8 sensors distributed over a finger-shape area (Fig 8(a)). A contact with a flat object such as an indenter ((b)) may activate 4 sensors at the same time (c). As described in the theoretical section, contact an object with the e-skin represents a dynamic process, involving different individual sensors at different time moments. The sequence of the activated sensors represents the tactile information about the sensors-object interaction in population. In order to investigate the sensing and coding in population, we have fabricated a series of objects by considering different combinations of nominal stiffness

This project has received funding from the European Union's Horizon 2020 research and innovation programme under grant agreement No 965044

and curvatures. By contacting the e-skin with the objects, population of spike trains encoding dynamic information was recorded and analysed by stochastic method. The result shows that the data samples are well grouped into categories characterized by the nominal stiffness and curvatures. Furthermore, using ML based on SNN, the tactile information encoded in the population of spike trains can be well decoded and further transformed to implement a classification task. This work is underway with an endeavour to shed light on the coding process and uncover the potential of our e-skin in real applications.

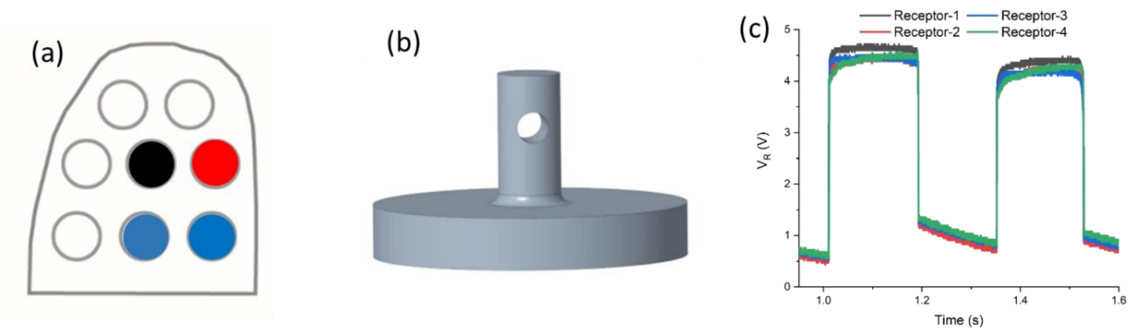

Fig. 8 An array of 8 sensors was fabricated in a finger-like area comprising a polyimide substrate, a patterned Cu film and a PDMS skin. Touching (b) the flat surface of an indenter activates (c) 4 sensors simultaneously.

3.2 Electrical characterizations of the e-skin integrated on MIA hand fingers

To provide tactile feedback to the human brain. A silicone matrix containing a hydrogel-based sensor array, known as e-skin, is mechanically integrated within the MIA hand fingers. This section describes the evaluation and electrical characterization of the e-skin with 6-14 sensors integrated into the MIA hand fingers.

3.2.1 Layout of sensors on the MIA fingers

Nine MIA fingers were characterized as received from SSSA. The nine MIA fingers can be grouped into thumb and index fingers with 6 or 14 individual sensing electrodes (see Table 1). Smooth-Sil™ 960, SmoothOn Inc (shore 60A) was chosen as the artificial skin covering the sensing electrodes. The fabrication method is described in *D4.3 – Fabrication of e-skin compatible with Mia hand*. In Table 1, the as-fabricated MIA fingers are labelled with serial numbers. The photos in Fig. 9 display the layout and position of each sensor on the fingers. By comparing the layout and dimensions from SSSA (Fig 10-15), the position of the sensors on the MIA fingers is pinpointed marked by colored dots (Fig 9).

This project has received funding from the European Union's Horizon 2020 research and innovation programme under grant agreement No 965044

Finger	Thumb			Index					
Serial number	A4	A5	B4	A9	A10	B6	B7	B8	B9
Sensor number	6	6	14	14	14	6	6	6	6

Table 1. Summary of the as-fabricated Mia hand fingers.

Fig 9. Photos of (a) front and (b) rear side of the as-fabricated Mia hand fingers integrated with e-skin where the blue/black dots mark the position of sensors inside the artificial skin used for electrical measurements.

This project has received funding from the European Union's Horizon 2020 research and innovation programme under grant agreement No 965044

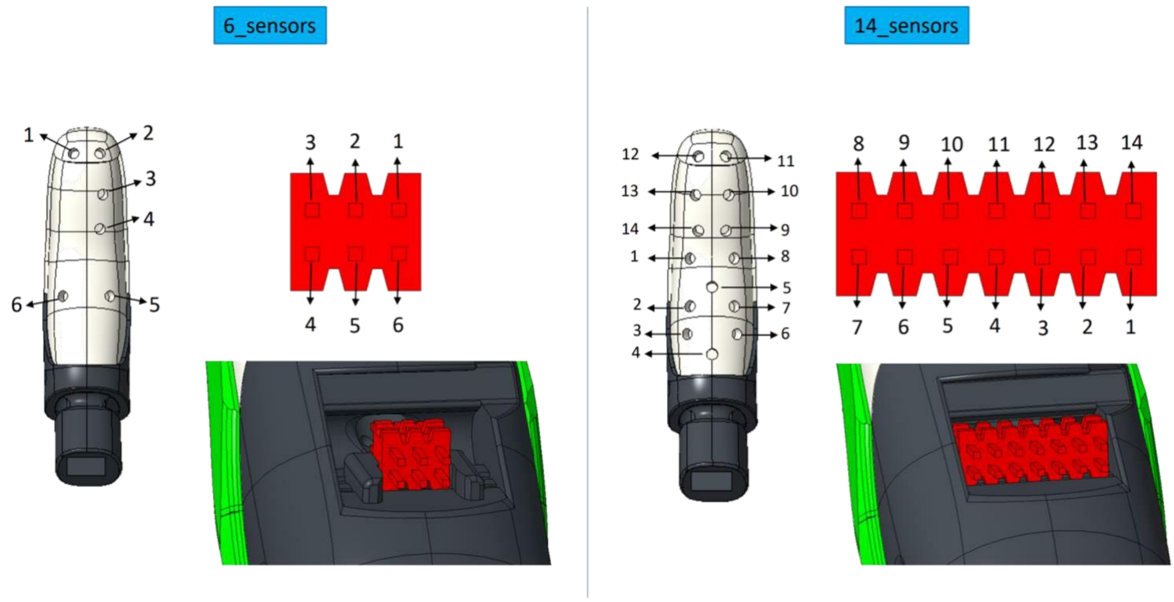

Fig 10. Layout of the sensors on Mia hand index fingers with 6 and 14 sensors, respectively.

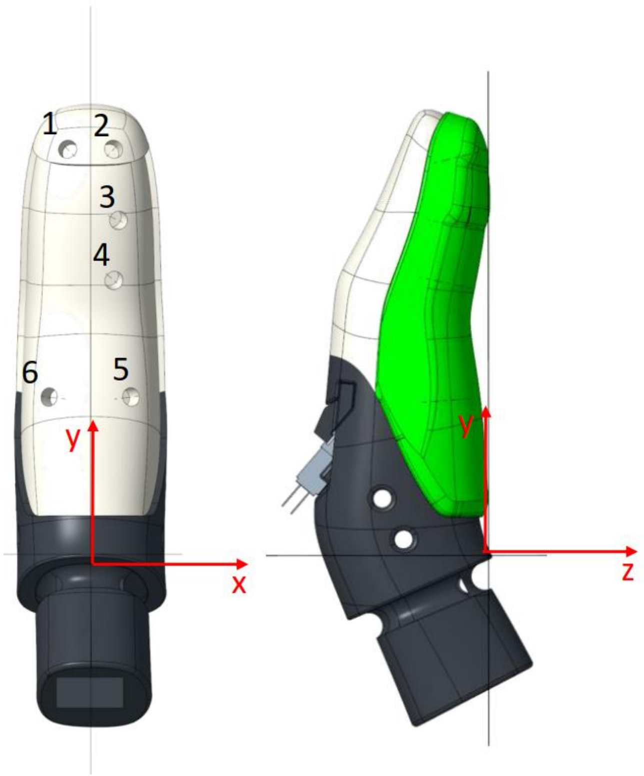

Sensor	X[mm]	Y[mm]
1	-2,5	44
2	2,5	44
3	3	35,5
4	2,5	29,5
5	4,3	16,5
6	-4,3	16,5

Fig 11. Position of the 6 sensors on Mia hand index.

This project has received funding from the European Union's Horizon 2020 research and innovation programme under grant agreement No 965044

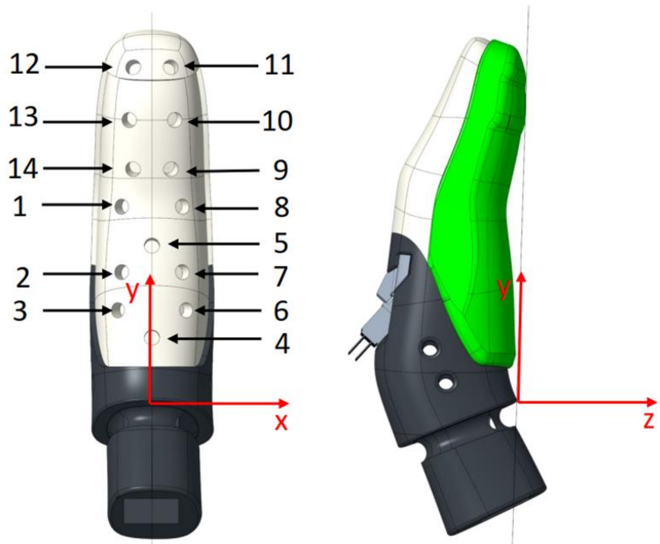

sensor	X[mm]	Y[mm]
1	-4	25,5
2	-4	17
3	-4,5	12
4	0	8,5
5	0	20,5
6	4,5	12
7	4	17
8	4	25,5
9	2,5	30,5
10	3	37
11	2,5	44
12	-2,5	44
13	-3	37
14	-2,5	30,5

Fig 12. Position of the 14 sensors on Mia hand index.

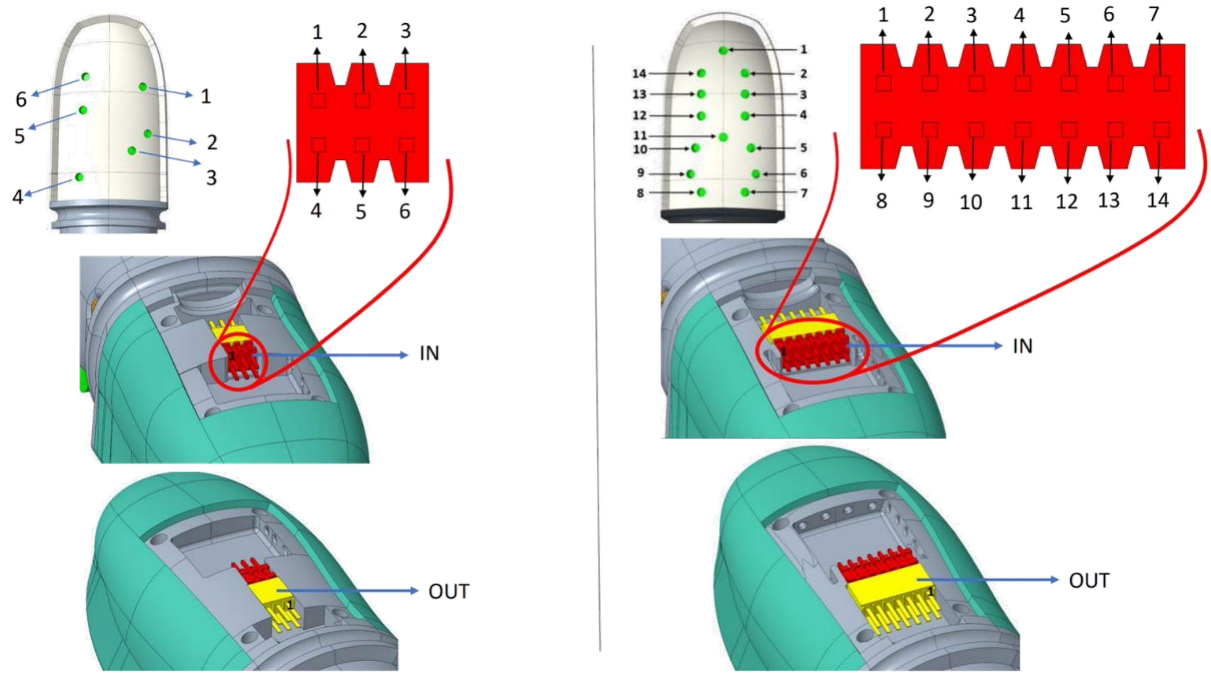

Fig 13. Layout of the sensors on Mia hand Thumbs with 6 and 14 sensors, respectively.

This project has received funding from the European Union's Horizon 2020 research and innovation programme under grant agreement No 965044

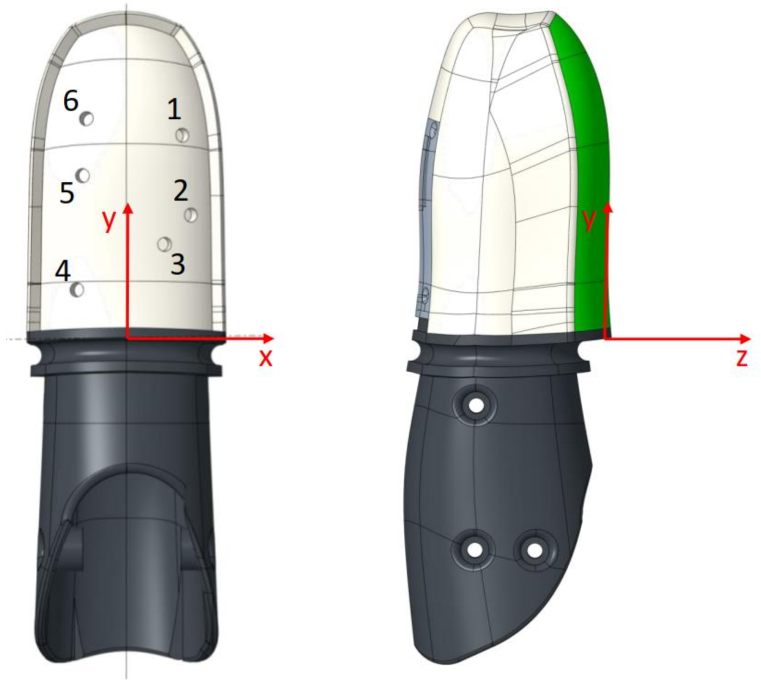

sensor	X[mm]	Y[mm]
1	8	29
2	9,5	18
3	5,5	13,5
4	-7,5	7,5
5	-6,5	23,5
6	-6	31,5

Fig 14. Position of the 6 sensors on Mia hand thumb.

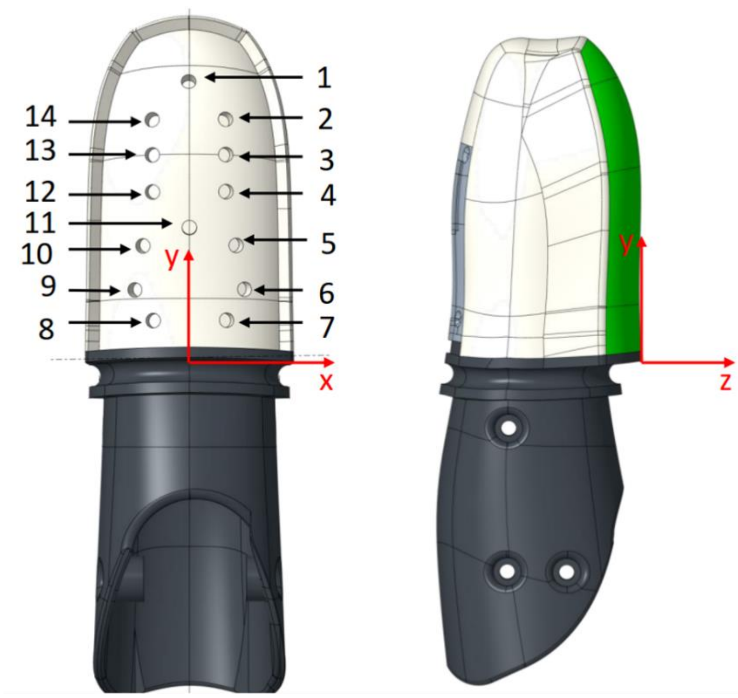

sensor	X[mm]	Y[mm]
1	0	38
2	5	33
3	5	28,5
4	5	23,5
5	6,5	16
6	7,5	10
7	5	6
8	-5	6
9	-7,5	10
10	-6,5	16
11	0	18,5
12	-5	23,5
13	-5	28,5
14	-5	33

Fig 15. Position of the 14 sensors on Mia hand thumb.

This project has received funding from the European Union's Horizon 2020 research and innovation programme under grant agreement No 965044

3.2.2 Electrical assessment of as-fabricated sensors on Mia hand fingers

To facilitate the evaluation and characterization of sensors on the MIA fingers, the fingers under assessment were mounted to finger holders received from SSSA (Fig 16). To initially test responsivity of each sensor on all as-received MIA fingers, output voltage in a response to touch of a human finger with the sensor was performed as shown in Fig. 17. The results showed that all sensors could respond to human touch and outputting voltage. To assess insulation between individual sensors and eliminate short-circuited sensors, resistance measurement between different sensors on the same finger was carried out using a multimeter. It was found that all sensors on Thumb B4 and A5, as well as Index B7 and B9 were well insulated from each other. However, some sensors on fingers Thumb A4 and Index A9 A10 B6 B8 have been electrically short-connected as illustrated in Fig 18. The resistance between the short-circuited sensors ranges from ~100 kΩ to ~1 MΩ, which indicates that the short connection was caused by conductive liquid between hydrogels rather than electrical wires. The cause of the short connection between neighbouring sensors will be further discussed in the following part *3.2.5 Robustness Evaluation of Sensors on Mia Hand*.

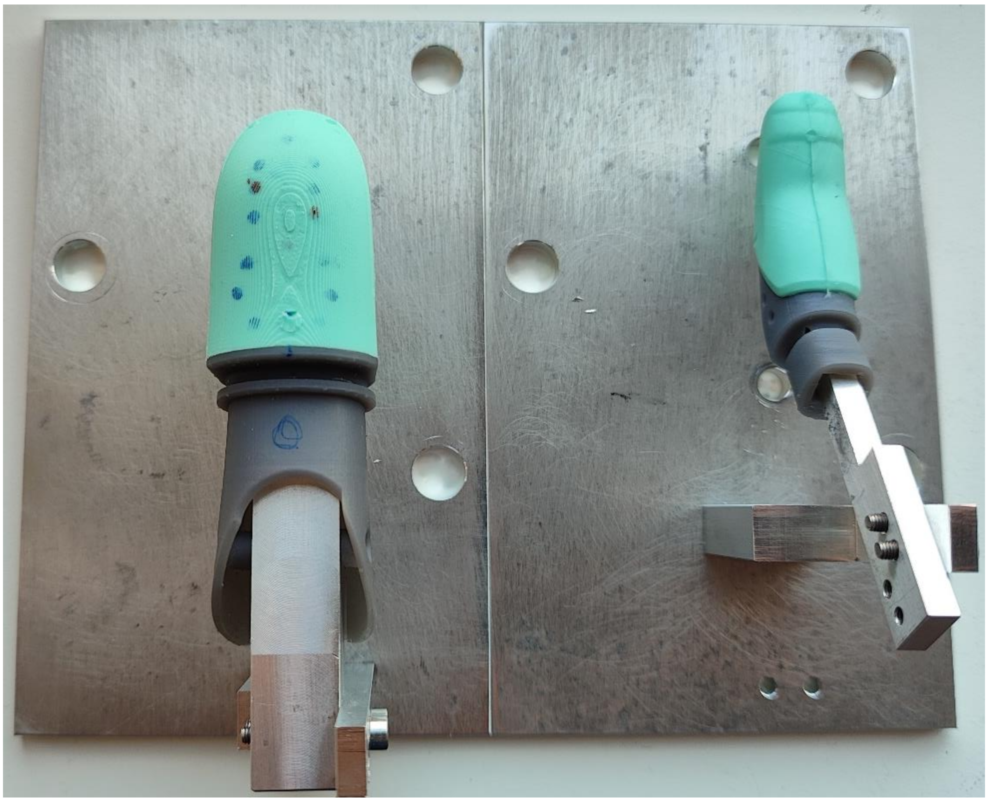

Fig 16. Mia hand fingers mounted on the holders for electrical assessment.

This project has received funding from the European Union's Horizon 2020 research and innovation programme under grant agreement No 965044

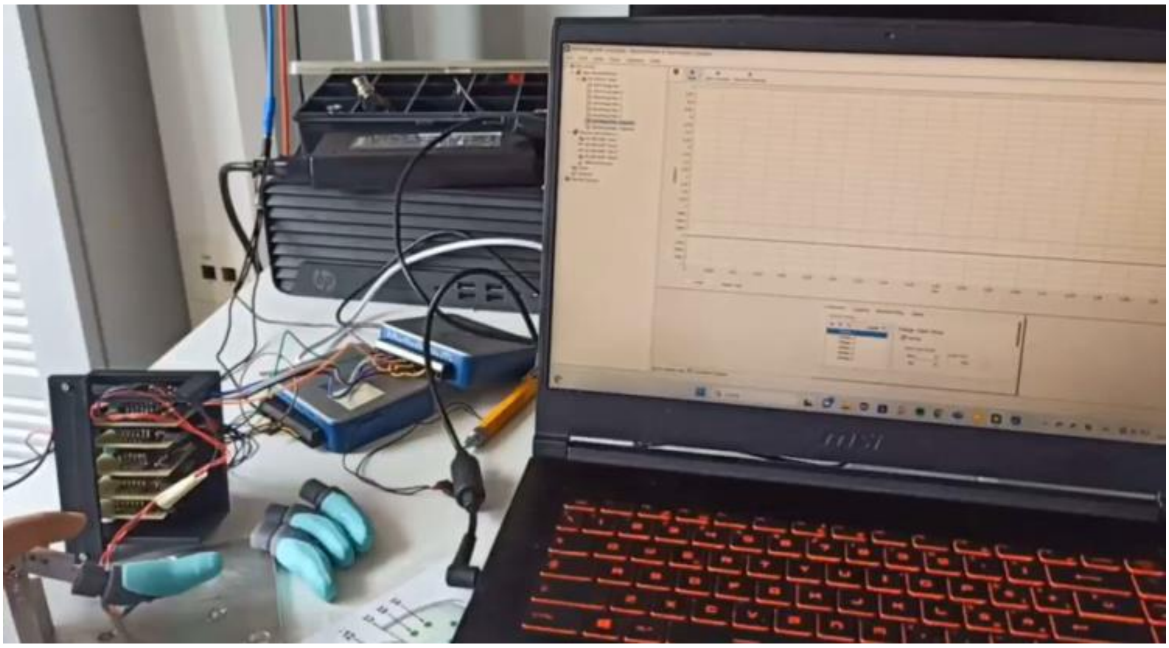

Fig 17. Initial evaluation of each sensor's output on Mia hand fingers.

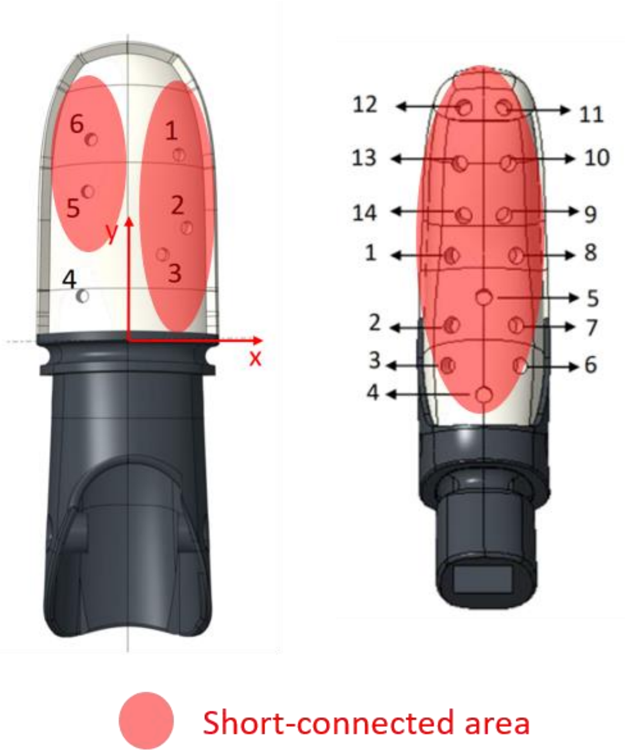

Fig 18. Illustration of the short connection between sensors on some Mia hand fingers.

3.2.3 Calibration of sensors on Mia hand fingers

As the sensors are analog in nature and prone to variabilities introduced by fabricating process to fill in hydrogels, contact with wires and so on, they need to be calibrated and adjusted beforehand in order to ensure a similar performance of the sensors in response to a similar stimulation. However, the curved surface of the Mia hand fingers poses a great

This project has received funding from the European Union's Horizon 2020 research and innovation programme under grant agreement No 965044

challenge to apply mechanical stimulations with the same force in the normal direction to different individual sensors distributed on a curved surface. In order to overcome this challenge, a new method was proposed to perform the sensor calibration. The method for the calibration relies on measuring the sensors' impedance using a Precision LCR Meter (HP HEWLETT 4284A, Fig 19 (A)). We assumed that every sensor having the same input impedance provides the same electrical outputs in response to the same mechanical stimulation. Based on this assumption, a calibration process is proposed as summarized below.

1) Making a finger as a capacitor:

   A layer of aluminium foil is covered conformally on the finger's surface which is used as an electrode. The wires connecting the sensing electrodes are used as the counter electrode (Fig. 19 (B)).

2) Setting up the precision LCR Meter (Fig. 19 (A)):

   2.1) Connecting coaxial cables to ports of the LCR Meter.

   2.2) Setting measuring mode to Cs-Rs mode, frequency to 1kHz, and voltage to 1V.

   2.3) Calibrating the LCR Meter with open, short, and load conditions, respectively.

   2.4) Measuring the capacitance and resistance of a standard capacitor (8.2 pF) and a resistor (320 kΩ) connected in series to double check the accuracy of the LCR Meter's measuring results.

3) Measuring sensors' impedance:

   Using the calibrated LCR meter, to measure each sensor's impedance on the same finger. The sensor's equivalent circuit is illustrated in Fig. 19 (C).

4) Calibrating sensors' impedance:

   Connecting the compensating capacitor and resistor in series to each sensor and adjusting the compensating components' capacitance and resistance in order to make sure each sensor on the same finger has the same capacitance and resistance within a reasonable range.

The calibration results of sensors on Thumb A5, B4 and Index B9 are displayed in Table 2-4, respectively.

This project has received funding from the European Union's Horizon 2020 research and innovation programme under grant agreement No 965044

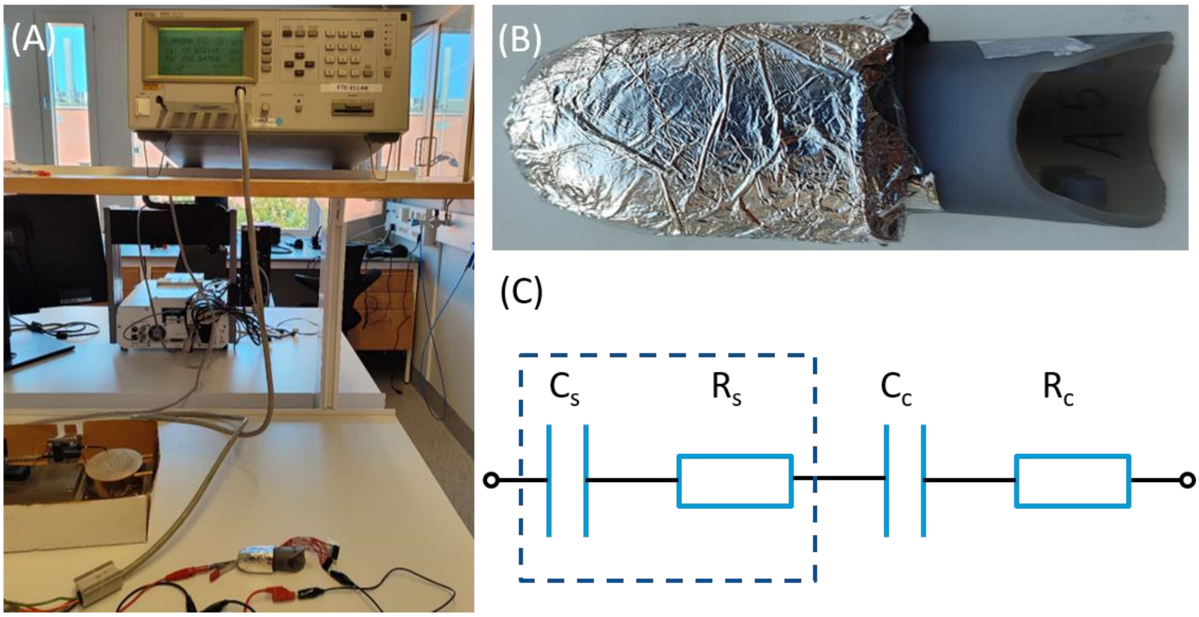

Fig 19. (A) Setup for calibration of sensors on Mia hand fingers. (B) An example of Mia hand thumb covered by a layer of Aluminium foil on the surface of silicone layer. (C) Illustration of the equivalent circuit of a sensor after calibration. Dashed box: equivalent circuit of an as-fabricated sensor before calibration. C_s and R_s are the capacitance and resistance of the as-fabricated sensor. C_c and R_c are the capacitor and resistor for calibration.

Sensor	Before calibration		Compensating components		After calibration	
	C_s (pF)	R_s (kΩ)	C_c (pF)	R_c (kΩ)	C (pF)	R (kΩ)
1	21.7	515	13.8	0	7.53	575
2	21.7	582	13.8	0	7.5	640
3	21.7	790	13.8	0	7.47	800
4	9.2	380	32.8	120	7.26	560
5	21.7	570	13.8	0	7.42	620
6	21.7	600	13.8	0	7.37	640

Table 2. Calibration table of sensors on Thumb A5.

This project has received funding from the European Union's Horizon 2020 research and innovation programme under grant agreement No 965044

Sensor	**Before calibration**		**Compensating components**		**After calibration**	
	C_s (pF)	**R_s (kΩ)**	**C_c (pF)**	**R_c (kΩ)**	**C (pF)**	**R (kΩ)**
1	16.1	235	16.4	270	7.54	600
2	16.17	248	16.4	270	7.54	600
3	16.5	283	16.4	270	7.67	630
4	7.87	570	0	0	7.87	570
5	13.24	975	24.6	0	7.5	950
6	7	540	0	0	7	540
7	13.4	534	24.6	82	7.5	560
8	6.14	640	0	0	6.14	640
9	6.93	570	0	0	6.93	570
10	11.56	804	32.8	0	7.28	770
11	11.54	440	32.8	120	7.27	550
12	11.5	440	32.8	120	7.32	600
13	7.05	680	0	0	7.05	680
14	16.56	322	16.4	270	7.8	600

Table 3. Calibration table of sensors on Thumb B4.

This project has received funding from the European Union's Horizon 2020 research and innovation programme under grant agreement No 965044

Sensor	Before calibration		Compensating components		After calibration	
	C_s (pF)	R_s (kΩ)	C_c (pF)	R_c (kΩ)	C (pF)	R (kΩ)
1	5.45	730	24.6	82	3.6	1000
2	5.43	640	24.6	82	3.6	1000
3	3.47	950	0	0	3.47	950
4	3.34	1000	0	0	3.34	1000
5	3.33	1000	0	0	3.33	1000
6	3.4	1000	0	0	3.4	1000

Table 4. Calibration table of sensors on Index B9.

3.2.4 Electrical characterizations of calibrated sensors on Mia hand fingers

After calibration, electrical characterizations of sensors on Mia hand fingers were performed.

1) The electrical characterization setup

A lab-built setup for electrical characterizations of sensors on Mia hand fingers in responses to mechanical stimulations was developed, as shown in Fig. 20. A Mia hand finger was mounted onto a finger holder. Sensors on the finger were connected to the analog-to-spike converter on a PCB board. The PCB board was powered by 5V and 3V output from a Dual Channel Output DC Power Supply (KEYSIGHT E3648A). Single sensor's output voltage and spike trains were recorded by the analogue channels of the Oscilloscope (Rigol MSO 5204). Output from the sensor array was recorded through the Oscilloscope's digital channels, which could record the spike trains from up to 16 sensors, simultaneously. A digital force gauge (Mxmoonfree 500N) was mounted on the movable terminal of a programmable linear motor (Zaber Technologies T-LSR300B), which was used to precisely control the movement (relative displacement, speed and acceleration) of the indenter on the tip of the force gauge and the force value applied on the finger. An indenter with a diameter of 15 mm was used to create contacts.

This project has received funding from the European Union's Horizon 2020 research and innovation programme under grant agreement No 965044

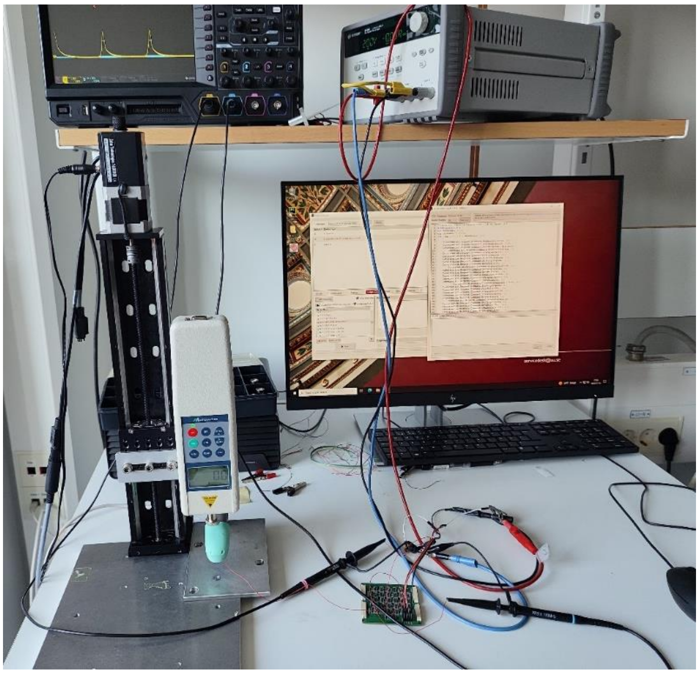

Fig 20. A lab-built setup for electrical characterizations of sensors on Mia hand fingers in response to mechanical stimulations.

2) Electrical characterization of sensors on the finger

To electrically characterize a sensor, the procedure below is followed.

a) For a marked sensor, place the sensor under the centre of the indenter.
b) Move the indenter to contact with the finger surface when the force is just 0 N and stop the movement.
c) Move the indenter upwards by 10 mm and set this position as the origin of the indenter.
d) Setup the displacement, speed (9.3 mm/s) and acceleration (1000 mm/s^2) of the movement of the indenter.
e) Move the indenter from the origin to press the finger surface with force increasing from 0 to 70 N and then return to the origin, which comprises 1 cycle of mechanical stimulation.
f) Repeat the mechanical stimulation for 10 cycles and record the sensor's output voltage and spike train simultaneously.

The typical output voltage and spike train of a single sensor on Mia hand finger (sensor 4 on Index B7) were displayed in Fig. 21. The result shows that the sensor responds well to the approaching process of contact. The analog-to-spike converter can auto-zero the sensor's output, thus eliminating environmental disturbance.

This project has received funding from the European Union's Horizon 2020 research and innovation programme under grant agreement No 965044

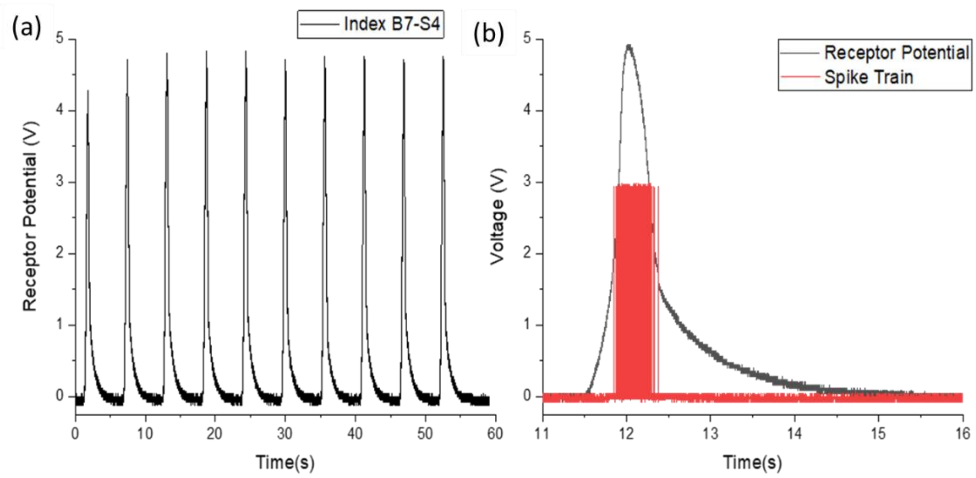

Fig 21. (a) Typical electrical output in voltage in response to repeating contacts and (b) the output in spike train (red) of a single sensor on a Mia hand finger.

3) Characterization of the sensor's response to contacts of varied applied force

To characterize the relation between the sensor's electrical output and the applied force and to identify the contact moment from the sensor's output, the applied force and the sensor's output were simultaneously recorded by the oscilloscope. For this purpose, the Shimadzu AGS was used as shown in Fig. 22 (a). The procedure is as below.

a) For a marked sensor, place the sensor under the centre of the indenter.
b) Move the indenter to contact with the finger surface when the force is just 0 N and stop the movement.
c) Move the indenter upwards by 10 mm and set this position as the origin of the indenter.
d) Setup the displacement, speed (9.3 mm/s) and acceleration (1000 mm/s^2) of the movement of the indenter.
e) Move the indenter from the origin to press the finger surface until reaches the targeted displacement, and then return to the origin, which comprises 1 cycle of mechanical stimulation.
f) Repeat the mechanical stimulation for 10 cycles and record the sensor's output voltage and spike train as well as the indenter's displacement and applied force simultaneously.
g) Increase the displacement of the indenter by 0.25 mm but keep the displacement no higher than 12 mm, which results in an increase in the largest force applied on the sensor, and repeat step d) to g).

The results are displayed in Fig. 22. It can be seen that the moment when the sensor's output voltage reaches the peak is just the contact moment that the force starts to increase from 0. It confirms that with the analog-to-spike converter, the sensor's output could be easily

This project has received funding from the European Union's Horizon 2020 research and innovation programme under grant agreement No 965044

used to determine the contact moment. Moreover, the sensor's output peak voltage increases with the applied final force from 0 to 70N.

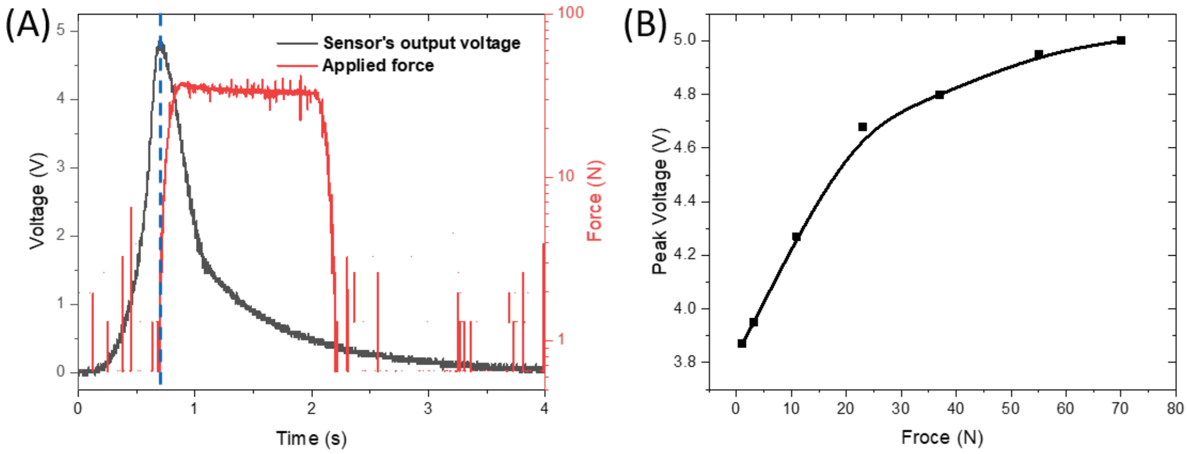

Fig 22. (A) Simultaneously recorded the sensor's output voltage and applied force on the sensor. The blue dashed line indicates the contact moment. (B) Sensor's output peak voltage to final contact force.

4) Characterization of the sensor's response to contacts of varied approaching speed

To characterize the influence of approaching speed of the indenter, the characterization procedure is as the following.

a) Set up the approaching speed of the indenter.
b) Move the indenter with the set speed to contact with the sensor and record its output.
c) Repeat the contact for 10 cycles and calculate the averaged peak voltage.
d) Change the approaching speed and repeat steps a) to c).

The results are displayed in Fig. 23. It can be seen that the sensor is sensitive to approaching speed. Its peak voltage increases quickly with speed. After installed on the Mia hand, the approaching speed of grasp can be easily controlled by Mia hand.

This project has received funding from the European Union's Horizon 2020 research and innovation programme under grant agreement No 965044

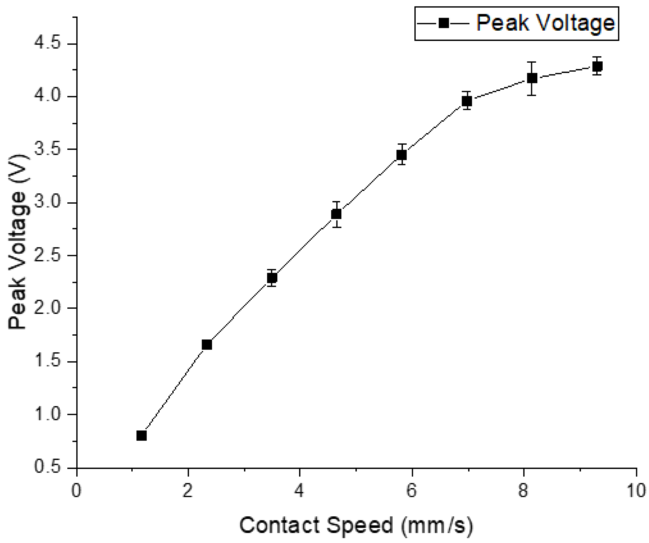

Fig 23. Electrical characterization of the sensor's output peak voltage to contact speed. Error bar: standard deviation of peak voltage.

5) Characterization of the sensor's response to contacts of varied materials

Sensor's outputs to different materials, often used in daily life including metal (aluminium), plastic (Kapton), paper, glass, and cloth, were then characterized. The characterization procedure is as below.

a) Cover the indenter with different materials in turn.
b) Set up the approaching speed of the indenter.
c) Move the indenter to contact with the sensor and record its output.
d) Repeat the contact for 10 cycles and calculate the averaged peak voltage.
e) Change the approaching speed and repeat steps b) to d).
f) Change the material and repeat steps a) to e).

The results are displayed in Fig. 24. It can be seen that at high approaching speed, the sensor's output peak voltage is similar for different materials. However, with relatively lower speeds, sensor's peak voltage differs from material to material. The results show that the sensor could not only responds well to the daily used materials but also possess the potential to classify the materials by its electrical output.

This project has received funding from the European Union's Horizon 2020 research and innovation programme under grant agreement No 965044

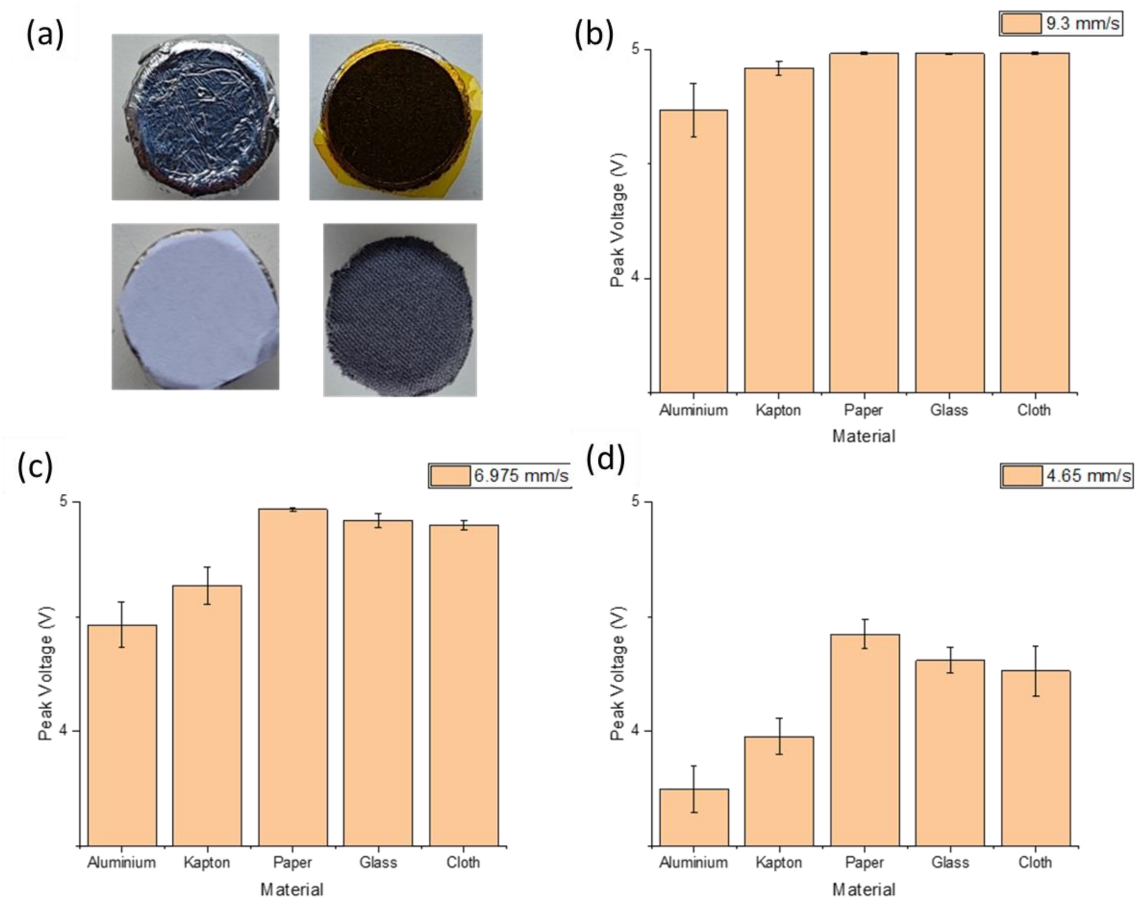

Fig 24. Electrical characterization of the sensor's response to contacting varied materials. (a) Images of indenter covered by a layer of (top left) Aluminium, (top right) Kapton, (bottom left) Paper, and (bottom right) cloth. (b-d) Sensor's output peak voltage, averaged of 10 cycles, for different materials with contacting speed ranging from 9.3 to 4.65 mm/s. Error bar: standard deviation of peak voltage.

3.2.5 Remaining challenge of integration of sensors in the skin of Mia hand fingers

To evaluate the robustness of sensors in the skin of Mia hand fingers, the resistance between sensors on the same finger, Thumb B4 and A5, as well as Index B7 and B9, was further checked after the sensor calibration and several rounds of electrical characterization. It turned out that the sensors on the fingers Thumb B4 A5 and Index B7 B9, which were insulated from each other before the calibration, were partly or all short-circuited after the characterization experiment. The resistance between different sensors on these fingers ranges from ~100 kΩ to ~1 MΩ. The sensor's output voltage has also been degraded. Fig. 25 (a) illustrates the evolution in the short connection during repeated mechanical stimulations.

To find the cause of the short connection, and check what happened inside the skin of the finger, we tried to cut the skin and found that the two layers of silicone (Smooth-Sil™ 960, SmoothOn Inc) did not adhere intimately. The top layer could be easily peeled off, as shown in Fig. 25 (b). There was a small gap between the top layer and the bottom layer. The

This project has received funding from the European Union's Horizon 2020 research and innovation programme under grant agreement No 965044

conductive liquid in hydrogel could spread easily between different hydrogels causing short connections, especially under pressure applied by repeated contacts. It confirms the previous assumption that the short connection is through conductive liquid between hydrogels other than electrical wires. The wires remain in good contact with hydrogels. No corrosion is observed. Hydrogel partly disappears and its colour changes from transparent to light green, similar to the colour of silicone, indicating chemical reactions between the hydrogel and dragon skin.

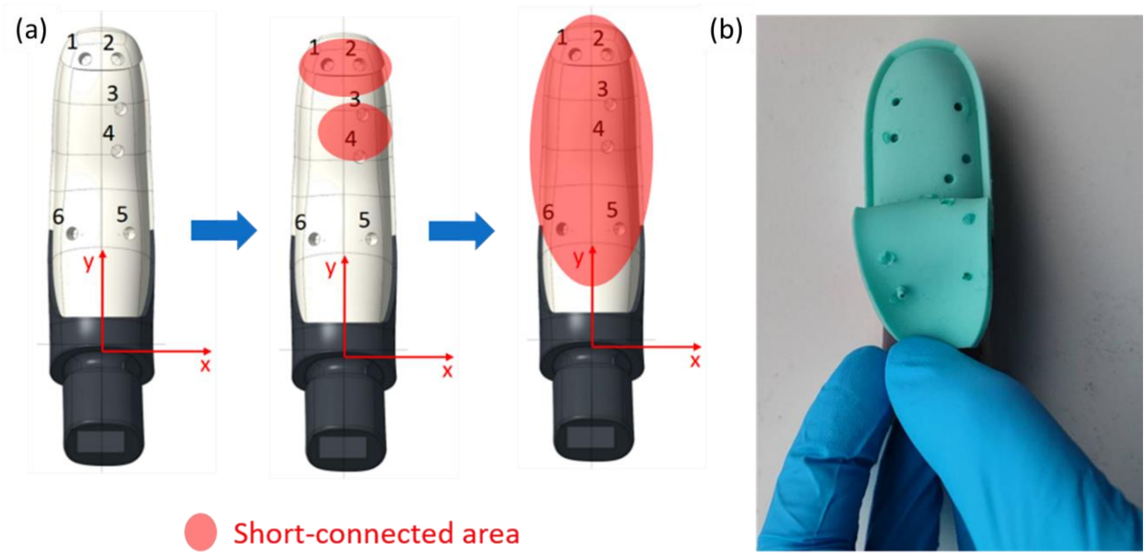

Fig 25. (a) Illustration of sensors on Mia hand fingers became short-connected after repeated contacts. (b) Image of the top layer of Mia finger peeled off from the bottom layer. Each hole on the finger denotes the position of a single sensor.

4 Revision history

REVISIONS			
Version #	**Date**	**Type of Change**	**Lead Author**
2	2023-09-18	Revision	Z.-B Zhang
3	2023-09-19	Revision	L. Chen
3	2023-09-20	Revision	Z.-B Zhang

This project has received funding from the European Union's Horizon 2020 research and innovation programme under grant agreement No 965044